Supporting Information

Solution plasma-cobalt hydroxide enabled nitrogen fixation

Yangwenting Ou[1], Jinglun Du[1], Changhua Wang, Qi Wu, Shuang Liang, He Ma, Xintong Zhang**

Key Laboratory of UV-Emitting Materials and Technology of Chinese Ministry of Education, Northeast Normal University, Changchun 130024, China

E-mail: wangch100@nenu.edu.cn; xtzhang@nenu.edu.cn

1. Experimental:

1.1 Experimental facility: A quartz plasma reactor, positioned above a magnetic stirrer, is equipped with one hollow metal tungsten electrode (inner diameter 1 mm, outer diameter 3 mm) and one solid metal tungsten electrode (diameter 3 mm). It also features a cooling circulation water system that can control the reaction temperature to 10 ℃. During the experiment, a nitrogen gas flow rate of 0.5 L min-1 is introduced into 120 ml of pure water through the end of the hollow metal tungsten electrode. The high-frequency pulsed plasma system used has an output voltage of ±3.5 kV, a frequency of 60 kHz, and a pulse width of 3 μs. Concurrently, the plasma power source is activated to apply pulsed high voltage across the "needle-to-needle" electrodes.

1.2 Materials: $Co(OH)_2$ (99.9% metal basis, Aladdin Reagents), $CoSO_4 \cdot 7H_2O$ (99.9% metal basis, Aladdin Reagents), Co_3O_4 (99.5%, Innochem Reagents), $Ni(OH)_2$ (61% Ni, Macklin Reagents), $Fe(OH)_3$: 5 mmol of $FeCl_3$ (99.9% metal basis, Aladdin) was dissolved in 50 ml of ultrapure water, and 20 mmol of KOH (95%, Aladdin) was dissolved in 50 ml of ultrapure water. Then, the fully dissolved $FeCl_3$ solution was poured into the KOH solution and stirred. After stirring for 30 minutes, the suspension was transferred into centrifuge tubes and centrifuged at 9000 r min^{-1} for 10 minutes. The supernatant was discarded, and the precipitate was washed twice. Finally, the centrifuge tubes were placed in an oven at 60 ℃ to dry, obtaining $Fe(OH)_3$ powder.

1.3 Synthesis of nanosized $Co(OH)_2$: 5 mmol of $CoSO_4 \cdot 7H_2O$ was dissolved in 30 ml of ultrapure water, and 0.1 mol of KOH was dissolved in 20 ml of ultrapure water. The

fully dissolved $CoSO_4$ solution was then poured into the KOH solution and stirred. After stirring for 30 minutes, the suspension was transferred into three 50 ml polytetrafluoroethylene autoclaves and hydrothermally treated at 100 ℃ for 8 hours. Afterwards, the suspension was poured into centrifuge tubes and centrifuged at 9000 r min^{-1} for 10 minutes. The supernatant was discarded, and the precipitate was washed twice. Finally, the centrifuge tubes were placed in an oven at 60 ℃ to dry, yielding $Co(OH)_2$ powder.

1.4 Measurement of NO_2^-, NO_3^-, and H_2O_2:

The concentrations of NO_2^- and NO_3^- in plasma-activated water were quantitatively analyzed using a Shimadzu Ion Chromatograph (LC-20AD) equipped with an IC-GA3 guard column and an IC-A3 analytical column. The Ion chromatograms of NO_2^- and NO_3^- were shown in Figure S2, the peak emergence time for NO_2^- was around 5 minutes, and its concentration was determined by inserting the peak area into the standard curve y=6.19677E-6x+0.00184. The peak emergence time for NO_3^- was around 6.7 minutes, and its concentration was determined using the standard curve y=6.70127E-6x+0.0093, with the concentration unit being mmol L^{-1}.

The concentration of H_2O_2 in plasma-activated water was quantitatively measured using a Shimadzu UV-Visible Spectrophotometer (UV2600) with a wavelength range of 190-900 nm. Three solutions were prepared: Solution A: 0.1 g of N,N-diethyl-p-phenylenediamine was dissolved in 10 mL of 0.05 mol L^{-1} sulfuric acid solution; Solution B: 0.01 g of peroxidase was dissolved in 10 mL of ultrapure water; Solution C: 0.1 mol L^{-1} Na_2HPO_4 solution and 0.1 mol L^{-1} NaH_2PO_4 solution were mixed in a volume ratio of 1:9 and stirred until homogeneous. 6 mL of Solution C was added to 100 μL of the sample, followed by the sequential addition of 100 μL of Solution A and Solution B, and the mixture was shaken to ensure uniform mixing. The absorbance data at a wavelength of 552 nm was inserted into the standard curve y=0.000387987x-0.04838 to obtain the concentration of H_2O_2, with the unit being μmol L^{-1}.

1.5 Characterization:

The voltage and current signals of liquid-phase plasma discharge were recorded using a GW Instek GDS-2202A digital oscilloscope equipped with a high-voltage probe

and an electromagnetic induction ring. The actual power P required for discharge was determined by plotting the I-V curve and integrating the curve. The energy consumed during the discharge process was then calculated using the formula Energy Consumption (J mol^{-1}) = P(W) * T(s) * n^{-1} (mol^{-1}).

The optical emission spectroscopy (OES) signals during the liquid-phase plasma discharge process were detected using an Ocean Optics spectrometer (NOVA-EX 400-001-5685). The concentration changes of H^+ in the solution were measured using a Mettler Toledo FE28-Standard pH meter (testing range 0.00-14.00, resolution 0.01, accuracy ±0.01). ESR measurements for DMPO-·OH and DMPO-·H signals were conducted on a Bruker EMXnano spectrometer (298 K, 9.63 GHz). X-ray diffraction patterns were collected using a Rigaku D/MAX-2500 with filtered Cu-Kα radiation to measure the crystal structure of the materials. The surface morphology and size of the materials were observed and measured using a JEOL JSM 4800F. The chemical composition and elemental states of the material surfaces were analyzed using XPS (Thermo SCIENTIFIC ESCALAB 250Xi), with the excitation source being Al target Kα radiation. The binding energy was calibrated using the C1s peak (284.8 eV) of adventitious carbon contamination. In-situ Infrared Spectroscopy measurements were performed using a Thermo Scientific Nicolet IS10 spectrometer. NO gas passed through water at a flow rate of 150 mL min^{-1} was introduced into the reactor to record the changes in the adsorption state of NO_x on the material surface at different times.

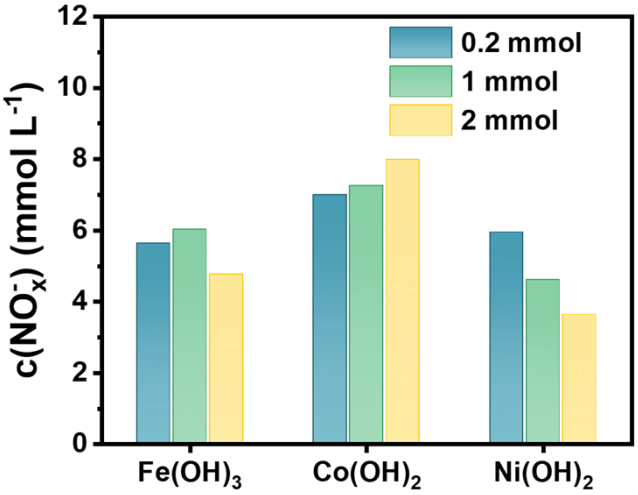

Figure S1. Concentrations of NO_x^- produced after 120 minutes of discharge with the addition of different doses of $Fe(OH)_3$, $Co(OH)_2$ and $Ni(OH)_2$.

We Added 0.2 mmol, 1 mmol and 2 mmol of metal hydroxides to the system respectively. It was found that $Co(OH)_2$ consistently exhibited the best nitrogen fixation performance when different doses of additives were added.

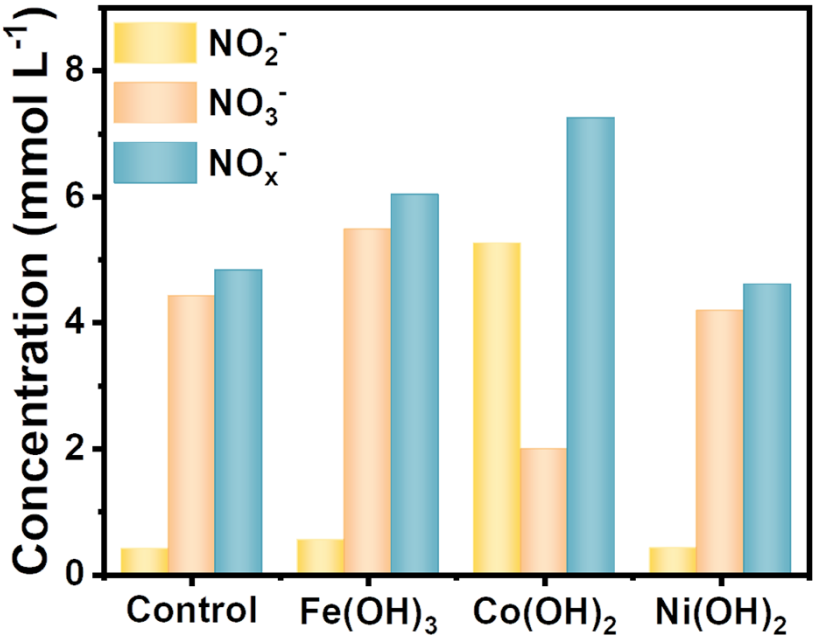

Figure S2. Concentrations of NO_2^-, NO_3^-, and NO_x^- produced after 120 minutes of discharge with the addition of 1 mmol of different metal hydroxides.

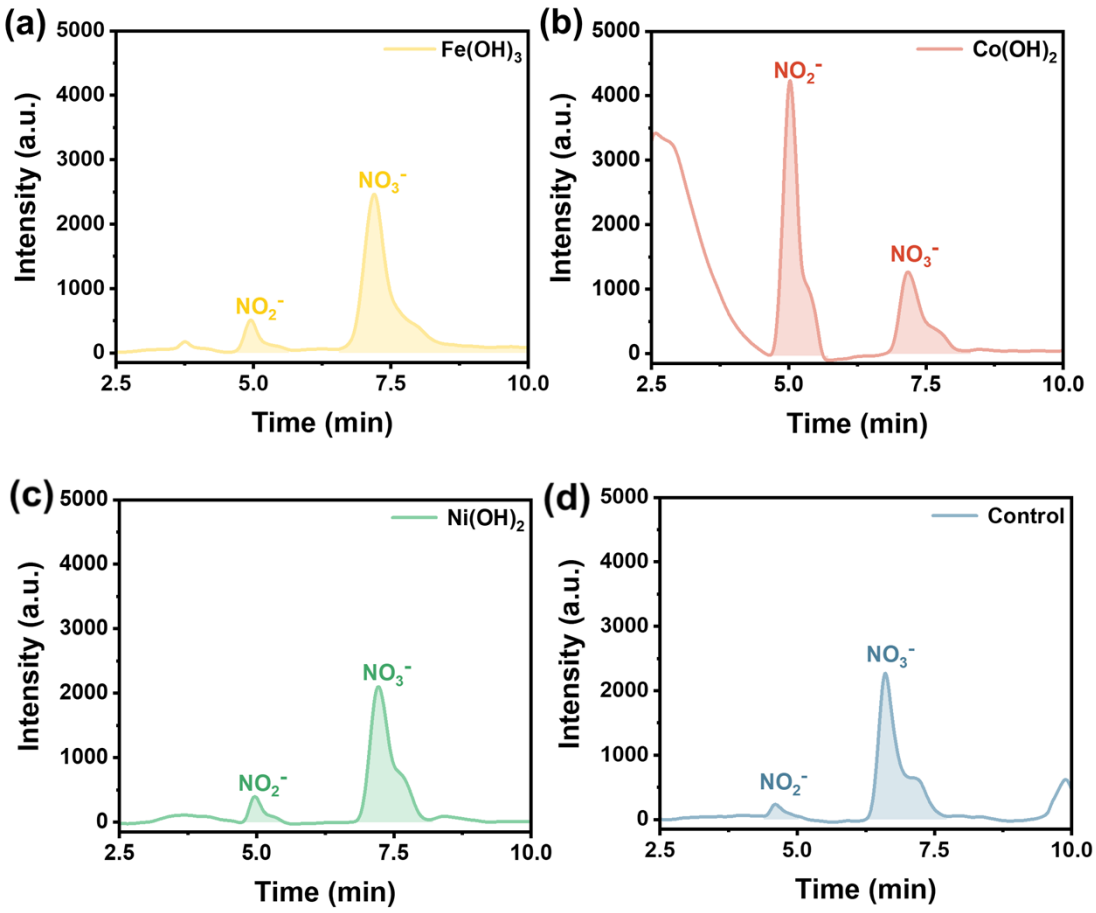

Figure S3. Ion chromatograms of NO_2^- and NO_3^- produced after 120 minutes of discharge with the addition of 1 mmol of (a) $Fe(OH)_3$, (b) $Co(OH)_2$, (c) $Ni(OH)_2$, and (d) in pure water.

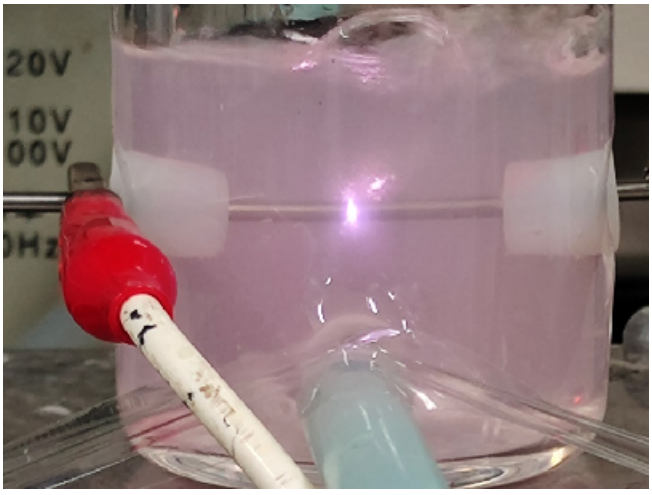

Figure S4. Pictures of the solution during discharge with the addition of 1 mmol $Co(OH)_2$.

Table S1. Ratios of each RNS and ROS peak to the reference peak (Hα).

	RNS 337 nm	RNS 355 nm	RNS 747 nm	RNS 868 nm	ROS 778nm	ROS 822nm
Control	0.01	0.01	0.04	0.12	0.46	0.11
$Ni(OH)_2$	0.12	0.00	0.09	0.28	0.49	0.21
$Fe(OH)_3$	0.09	0.01	0.08	0.3	0.6	0.17
$Co(OH)_2$	0.18	0.04	0.15	0.51	0.57	0.26

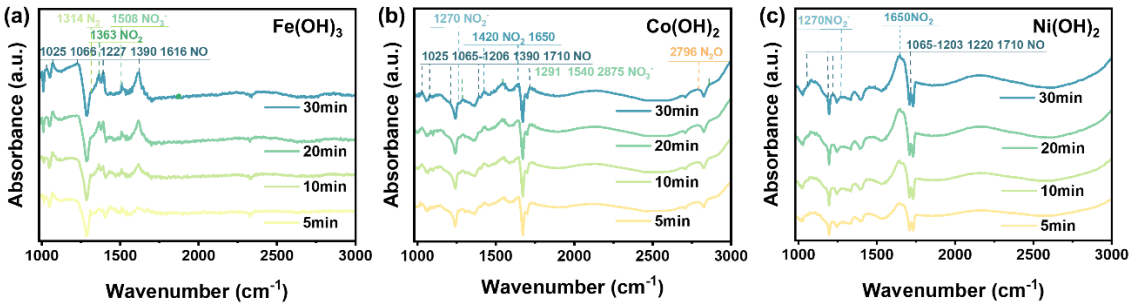

Figure S5. In-situ infrared spectra of (a) $Fe(OH)_3$, (b) $Co(OH)_2$, (c) $Ni(OH)_2$.

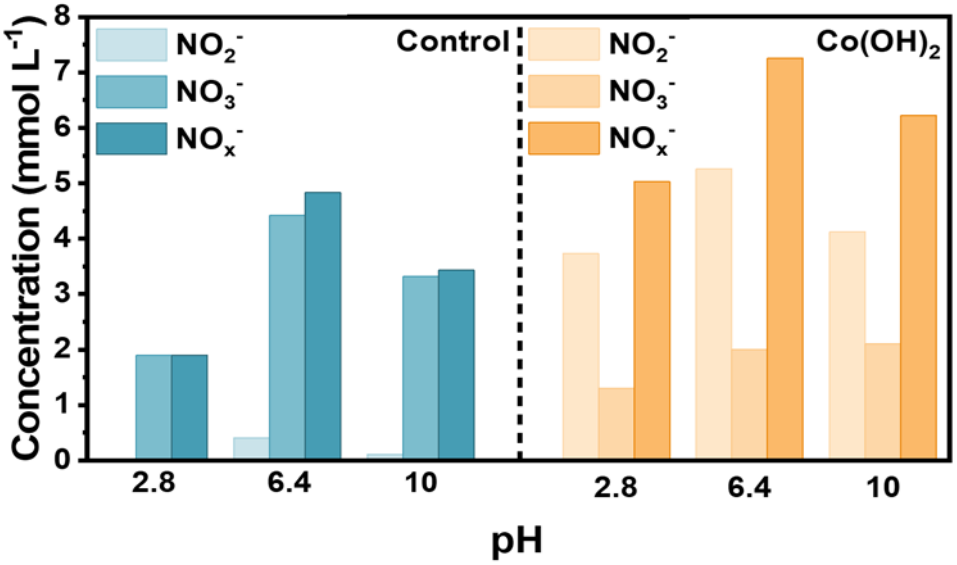

Figure S6. Concentrations of NO_2^-, NO_3^-, and NO_x^- produced after 120 minutes of discharge in pure water and with the addition of 1 mmol $Co(OH)_2$ at different initial pH values.

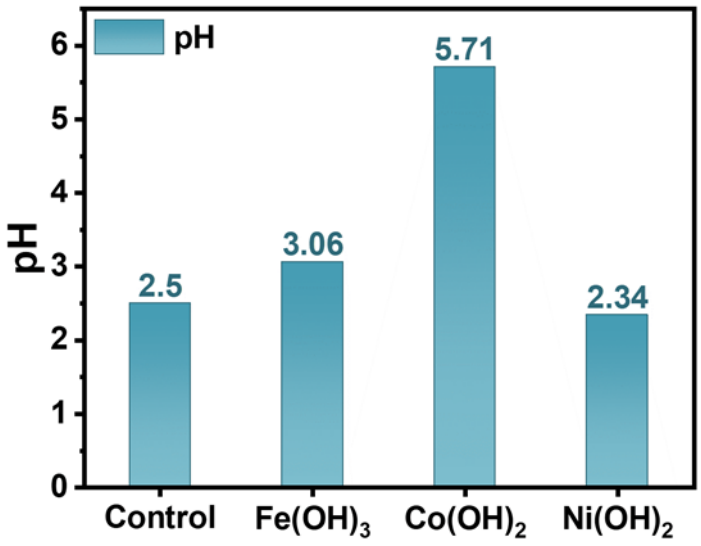

Figure S7. pH values after discharge in pure water and with the addition of 1 mmol of various catalysts.

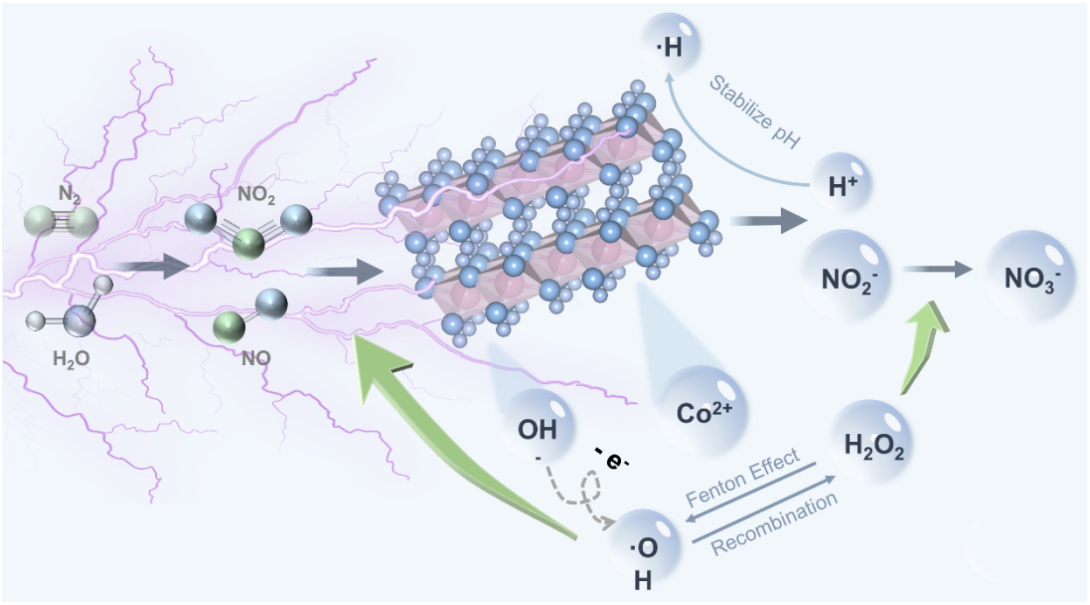

Figure S8. Mechanism diagram for the promotion of nitrogen fixation by $Co(OH)_2$.

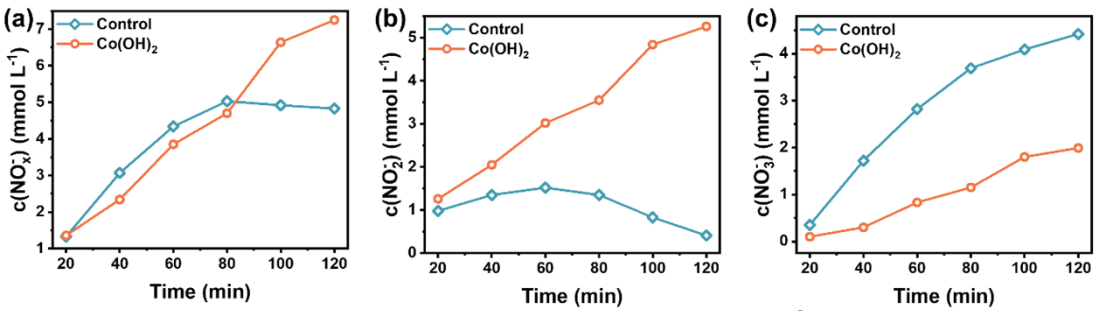

Figure S9. Changes in the concentrations of (a) NO_x^-, (b) NO_2^- and (c) NO_3^- within 120 min with the addition of 1 mmol $Co(OH)_2$ discharge.

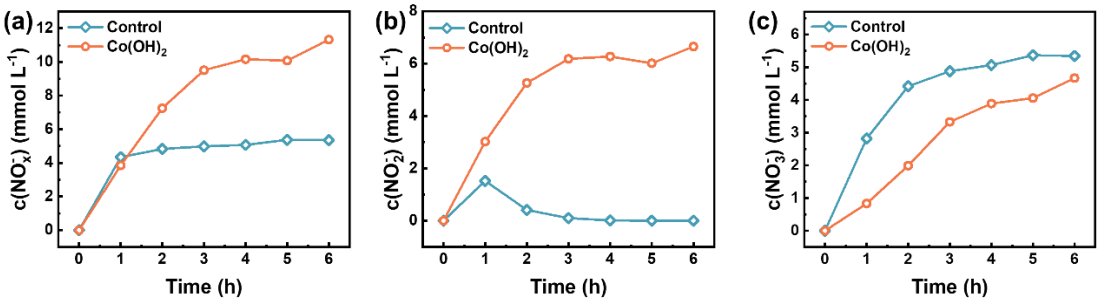

Figure S10. Changes in the concentrations of (a) NO_x^-, (b) NO_2^- and (c) NO_3^- within 6 h with the addition of 1 mmol $Co(OH)_2$ discharge.

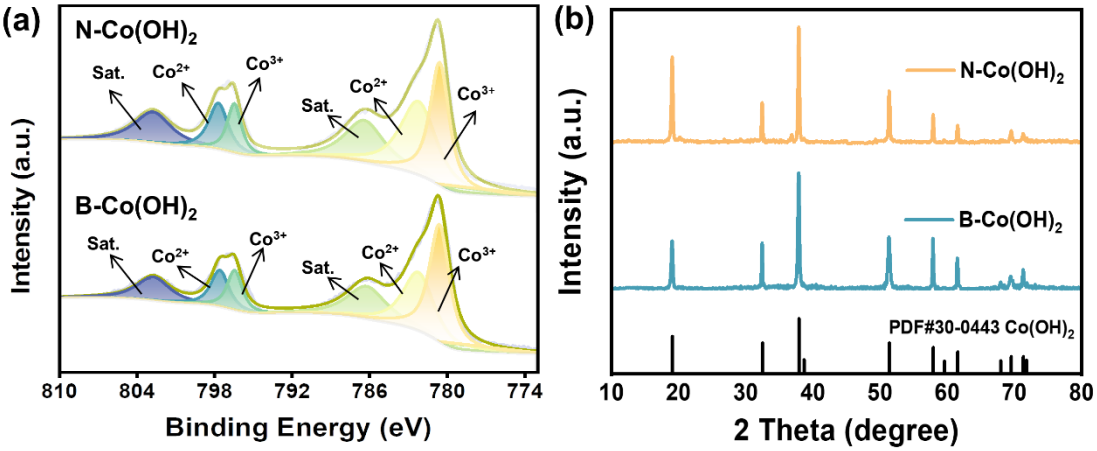

Figure S11 (a) XPS spectra comparison between N-$Co(OH)_2$ and B-$Co(OH)_2$, (b) XRD comparison between N-$Co(OH)_2$ and B-$Co(OH)_2$.

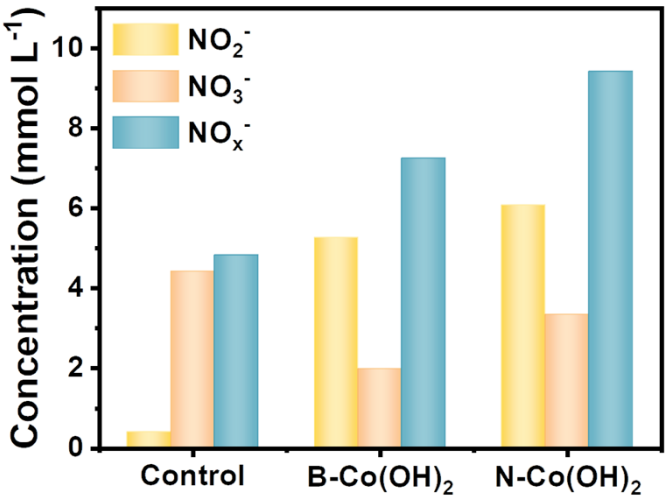

Figure S12. Concentrations of NO_2^-, NO_3^-, and NO_x^- produced after 120 minutes of

discharge with the addition of 1 mmol of B-$Co(OH)_2$ and N-$Co(OH)_2$.

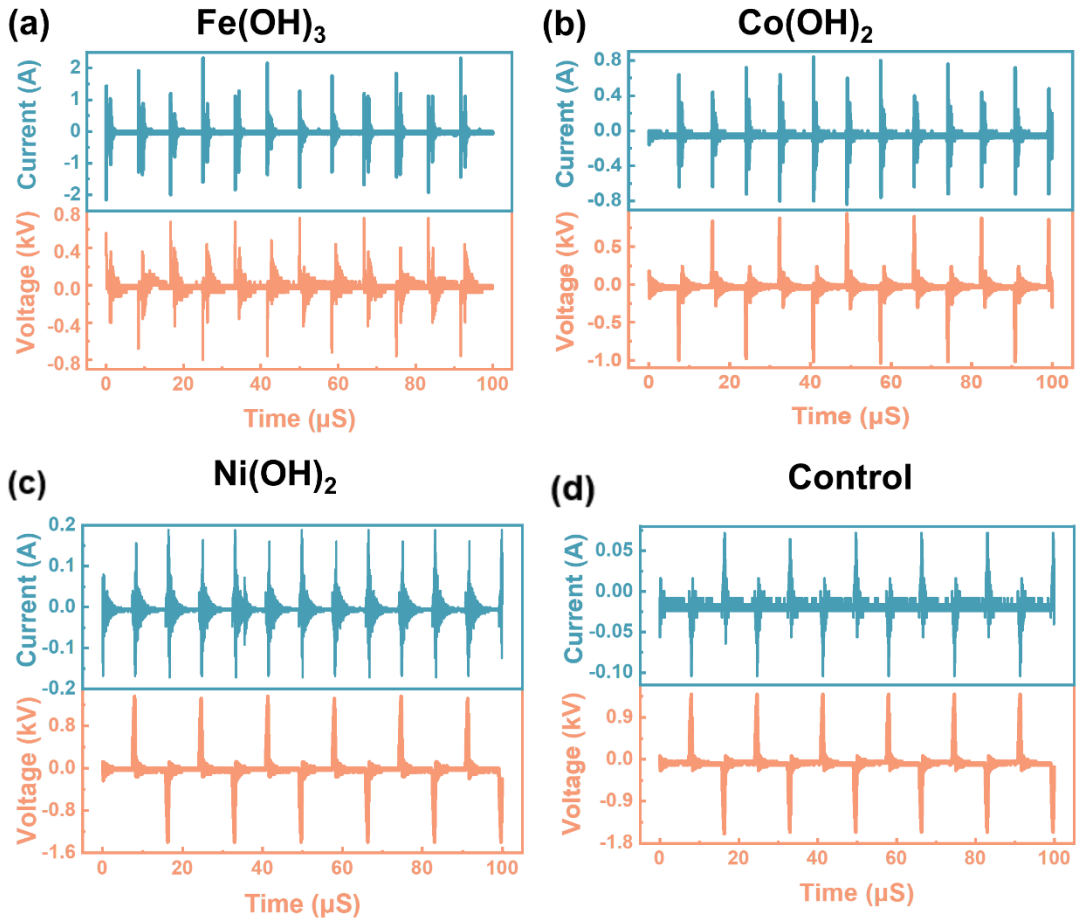

Figure S13. I-V curves during discharge with the addition of 1 mmol of (a) $Fe(OH)_3$, (b) $Co(OH)_2$, (c) $Ni(OH)_2$ and (d) in pure water.

Table S2. The actual power P during discharge.

	Control	$Fe(OH)_3$	$Co(OH)_2$	$Ni(OH)_2$
Power	7.46 W	5.66 W	4.21 W	5.82 W

Table S3. A comparison of NO_x^- production rates between this work and other studies.

	Catalyst	Production rate (μmol g^{-1} h^{-1})
Photocatalysis	Pd/H-TiO_2	4.58 [1]
	WO_3/CdS	14.2 [2]
	Pothole-rich WO_3	32 [3]
	TiO_2/WO_3	160 [4]
Electrocatalysis	Ru-doped TiO_2/RuO_2	161.9 [5]
	Rh	168 [6]
	AD-Fe NS	6120 [7] (2.45 μmol cm^{-2} h^{-1})
	Ru-doped Pd	77.7 [8]

This Work	$Co(OH)_2$	6077.42 (6280 μmol cm^{-2} h^{-1})

References:

1. X. Zhang, R. Shi, Z. Li, J. Zhao, H. Huang, C. Zhou and T. Zhang, *Adv. Energy Mater.*, 2022, **12**, 2103740.
2. P. Xia, X. Pan, S. Jiang, J. Yu, B. He, P. M. Ismail, W. Bai, J. Yang, L. Yang, H. Zhang, M. Cheng, H. Li, Q. Zhang, C. Xiao and Y. Xie, *Adv. Mater.*, 2022, **34**, 2200563.
3. Y. Liu, M. Cheng, Z. He, B. Gu, C. Xiao, T. Zhou, Z. Guo, J. Liu, H. He, B. Ye, B. Pan and Y. Xie, *Angew. Chem. Int. Ed.*, 2019, **58**, 731-735.
4. Y. Yu, C. Wang, Y. Yu, Y. Huang, C. Liu, S. Lu and B. Zhang, *J. Mater. Chem. A*, 2020, **8**, 19623-19630.
5. M. Kuang, Y. Wang, W. Fang, H. Tan, M. Chen, J. Yao, C. Liu, J. Xu, K. Zhou and Q. Yan, *Adv. Mater.*, 2020, **32**, 2002189.
6. T. Li, S. Han, C. Cheng, Y. Wang, X. Du, Y. Yu and B. Zhang, *Angew. Chem. Int. Ed.*, 2022, **61**, e202204541.
7. Y. Guo, S. Zhang, R. Zhang, D. Wang, D. Zhu, X. Wang, D. Xiao, N. Li, Y. Zhao, Z. Huang, W. Xu, S. Chen, L. Song, J. Fan, Q. Chen and C. Zhi, *ACS Nano*, 2022, **16**, 655-663.
8. T. Li, S. Han, C. Wang, Y. Huang, Y. Wang, Y. Yu and B. Zhang, *ACS Catal.*, 2021, **11**, 14032-14037.